

## A RE-EXAMINATION OF OBSERVED AND PREDICTED STELLAR IONIZING FLUXES IN THE LARGE MAGELLANIC CLOUD

E. S. VOGES<sup>1</sup>, M. S. OEY<sup>2</sup>, R. A. M. WALTERBOS<sup>1</sup>, AND T. M. WILKINSON<sup>2</sup>

<sup>1</sup> Department of Astronomy, New Mexico State University, P.O. Box 30001, MSC 4500, Las Cruces, NM 88003, USA

<sup>2</sup> Department of Astronomy, University of Michigan, 830 Dennison Building, Ann Arbor, MI 48109-1042, USA

Received 2007 August 31; accepted 2008 January 21; published 2008 March 6

### ABSTRACT

We use  $H\alpha$  luminosities of H II regions in the Large Magellanic Cloud to test the latest generation of hot-star atmosphere models. These newer models predict softer spectral energy distributions, and imply that less ionizing radiation escapes from classical H II regions than found in our previous study. Our analysis is based on a sample of 14 objects that have comprehensive inventories of spectroscopic classifications for the ionizing stars, and we also present a larger sample of 39 objects for which stellar properties are more roughly estimated from broadband photometry. Although the latter sample offers crude constraints, the results are fully consistent with, and support those from, the former sample. We find that the latest stellar atmosphere models predict that only 20–30% of H II regions are density bounded. This is consistent with the shell-like and filamentary morphology seen in those candidates. With these results, the total photon budget may not provide enough Lyman continuum radiation to account for the diffuse, warm ionized medium.

*Key words:* galaxies: ISM – H II regions – ISM: general – Magellanic Clouds – stars: atmospheres – stars: early-type

### 1. INTRODUCTION

The ionizing radiation from massive stars is a feedback mechanism of vital importance to a wide variety of astrophysical processes, including star formation, galaxy evolution, and cosmic re-ionization. Yet, on a quantitative level, the ionizing photon emission rates are still relatively uncertain, as a function of specific stellar parameters. Models of these complex, non-LTE stellar atmospheres have improved dramatically during the last two decades, but empirical tests of these models remain few. Photoionized nebulae offer a classical test of stellar atmosphere models (e.g., Morton 1969) by offering an essentially direct measure of the Lyman continuum photon emission rates from the parent star. Oey & Kennicutt (1997; hereafter OK97) compared observed and predicted H II region luminosities for 14 OB associations in the Large Magellanic Cloud (LMC), and Hunter & Massey (1990) compared observed and predicted ionization rates for 30 Galactic H II regions, based on  $H\alpha$  and/or radio continuum observations. One complication for empirical tests is the variation in properties of individual stars. Thus, tests carried out for larger samples offer a broader evaluation of the models. For example, Hoopes & Walterbos (2000) used *HST* FUV–optical photometry of OB stars in M33 to derive predicted ionizing luminosities for H II regions and the field population. The goals of this current study are twofold: to evaluate more recent stellar atmosphere models and their predictions for stellar Lyman continuum emission rates; and to increase the sample of objects for which this comparison between observations and predictions has been made.

The results directly affect our understanding of the diffuse, warm ionized medium (WIM), a ubiquitous component of the interstellar medium in star-forming galaxies. What is the role of massive field stars in ionizing the WIM, relative to massive stars in OB associations? The WIM tends to have brighter emission near H II regions (Hoopes et al. 1996; Ferguson et al. 1996), suggesting that leakage of ionizing photons from nebulae may be an important contributor. Our global study of an external

galaxy’s H II regions is an important step toward understanding the fate of ionizing photons.

Earlier, we found that for some H II regions, the  $H\alpha$  luminosity predicted from the observed stellar content is higher than the observed  $H\alpha$  luminosity (OK97). This implies that those H II regions are density bounded and that ionizing radiation escapes from them. An inhomogeneous medium complicates matters because if we consider that the medium may have pockets of low-density gas, the distance over which ionization and recombination rates balance will vary. One can see that where regions of low-density gas exist, there will be pockets where the photons can travel further and ionize hydrogen beyond the classical Strömgen radius, or possibly escape from the local region altogether.

The concept of leaky H II regions has helped reconcile our models of H II regions, stellar atmospheres, and the WIM. However, the percentage of H II regions that may be leaky is not well determined. In their study of 14 H II regions in the LMC, OK97 found the ratio of the observed-to-predicted  $H\alpha$  luminosity to be  $<0.70$  for six of them. Hoopes & Walterbos (2000) noted that the two regions in OK97 that were leaking the most photons both had a ring-like morphology, prompting an exploration of the relation between H II region morphology and the leakiness. Hoopes and Walterbos classified the H II regions in M33 as either compact (center-brightened and discrete) or diffuse (filamentary or ring-like), but their results did not reveal a strong trend with morphology.

### 2. IONIZATION RATES FROM DIFFERENT MODELS

There are still significant variations in the predictions for Lyman continuum emission rates among different sets of model stellar atmospheres. Figure 1 shows the H-ionizing photon emission rate  $Q^0$  as a function of stellar spectral type. The heavy and light lines denote dwarfs and supergiants, respectively. We compare predictions by Martins et al. (2005; hereafter MSH), Smith et al. (2002; hereafter SNC), Schaerer & de Koter (1997; hereafter SdK), Vacca et al. (1996; hereafter VGS),

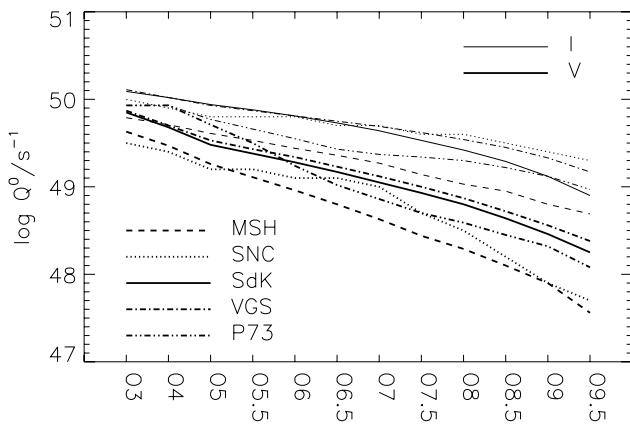


**Figure 1.** Comparison of ionizing photon emission rates for O V stars (heavy lines) and O I stars (light lines). Line types correspond to different sets of model atmospheres as shown. Values for some spectral types for SNC and P73 are interpolated or extrapolated (see the text).

and Panagia (1973; hereafter P73). Most of these predictions have been widely used and they are representative of the continuing progress in addressing the complexities of hot-star atmospheres. In particular, the emitted spectral energy distributions are produced by conditions that include expanding winds, non-LTE effects, and metal line-blanketing. The latter is especially complex, and various methods of approximating the radiation transfer in these millions of transitions have been applied through the years.

Since some authors provided only models for solar metallicity, all of the models considered here assume the solar value. The effects of metallicity have been discussed in several studies (e.g., Mokiem et al. 2004; Kudritzki 2002; MSH), which demonstrate that H-ionizing fluxes themselves do not vary significantly with metallicity for a given  $T_{\text{eff}}$ . However, recent studies show that the effective temperature scales are hotter for the Magellanic Clouds (e.g., Massey et al. 2005; Mokiem et al. 2006): roughly 4000 K for the Small Magellanic Cloud (SMC), while the LMC is closer to the Galactic scale, although other work (Heap et al. 2006) shows some uncertainty in this trend. The smaller stellar radii of lower-metallicity stars may offset the increase in  $Q^0$  due to higher  $T_{\text{eff}}$ , but the pattern is unclear at present (Mokiem et al. 2007; Heap et al. 2006). In any case, effects of the temperature scale that cause variations from Galactic estimates of  $Q^0$  are small for the LMC as compared to the SMC.

The ionizing fluxes from P73 have held up remarkably well over a quarter century, even though they are derived from model stellar atmospheres that are crude by modern standards. For stars of type O7.5 V and later, P73's ionizing fluxes are based on LTE model atmospheres calculated by Bradley & Morton (1969) and Van Citters & Morton (1970), which include basic line-blanketing by 110 major lines. For supergiants and hotter dwarfs, P73 adopts non-LTE models calculated by Auer & Mihalas (1972) without any line opacities included. None of these early models account for extended, expanding atmospheres. Predicted  $Q^0$  from the work by VGS are an updated version of this approach, and are derived from LTE, line-blanketed atmospheres by Kurucz (1992). While the line absorption is addressed in far greater detail, these models also omit the wind effects. On the other hand, the CoSTAR predictions of SdK made a first attempt to make at least some accommodation for all three effects, winds, NLTE, and line-blanketing, applying approximations for the winds and line-blanketing. The  $Q^0$ 's

more recently predicted by SNC are derived from models calculated with the WM-BASIC code (Pauldrach et al. 2001), which is one of the most physically realistic stellar atmosphere codes, explicitly accounting for all of the effects discussed. SNC incorporated their  $Q^0$  predictions into the popular STARBURST99 population synthesis code (Leitherer et al. 1999). Finally, MSH compute their Lyman continuum emission rates from atmospheres computed with the CMFGEN code (Hillier & Miller 1998), which is similarly sophisticated. WM-BASIC computes a hydrodynamical wind model, but does not compute the line transfer in the comoving frame, whereas CMFGEN does include the comoving frame, but with a simple wind velocity law and fewer explicit line transitions. Aggregate line transitions are treated with an opacity-sampling technique by WM-BASIC and a method of super-levels by CMFGEN. These and other atmosphere codes have been compared frequently in the literature, including in all of the works cited above, and others (e.g., Mokiem et al. 2004; Morisset et al. 2004; Lanz & Hubeny 2003).

These various studies derive their predicted ionizing emission rates not only on different atmosphere models, but also on different spectral-type- $T_{\text{eff}}$  relations and calibrations of fundamental stellar parameters. One can either directly match observed stellar spectra and SEDs to atmosphere models, or use models that are internally self-consistent between spectral type,  $T_{\text{eff}}$  and  $\log g$ . P73, VGS, and SNC used empirical calibrations, while SdK used theoretical parameters from their own stellar structure models. These CoSTAR models were the first to be fully self-consistent between the stellar models and atmosphere models. The MSH predictions considered here are those based on their "theoretical scale" models, which do include an empirical  $T_{\text{eff}}-\log g$  calibration. We note that they also present models based on an "observational scale," which results in somewhat higher  $Q^0$  predictions, with the largest difference from the theoretically-derived values occurring for the latest spectral types (see MSH for a detailed discussion of these differences). The SNC models are probably the most widely used, since they are included in the *Starburst99* population synthesis code (SNC; Leitherer et al. 1999). Users should note that these predictions are based on the somewhat outdated effective temperature scale of Crowther (1998).

Figure 1 shows that for dwarf O stars, the two recent studies by SNC and MSH generally predict softer ionizing SEDs than the earlier works. Furthermore, the MSH models are softer than all of the other models for supergiants as well. Both improvements in the atmosphere models and updated fundamental calibrations contribute to these effects. For the atmosphere models, advanced treatment of metal line-blanketing and winds more fully accounts for the UV opacities. At the same time, these results confirm other recent studies (e.g., Repolust et al. 2004; Bianchi & Garcia 2002) pointing to a significant shift (several 1000 K) toward cooler values in the  $T_{\text{eff}}$  scale. We refer the reader to the cited works for comprehensive discussions of these issues.

### 2.1. H II Regions With Stellar Spectral Classifications

Since massive star feedback is a collective effect resulting from numerous stars, it is revealing to examine the model-dependence of the total predicted ionizing emission rates for individual H II regions. To study the differences resulting from using different stellar atmosphere models, we re-analyzed the 14 H II regions examined by OK97, using the same spectroscopic classifications and extinction corrections they used, but now also

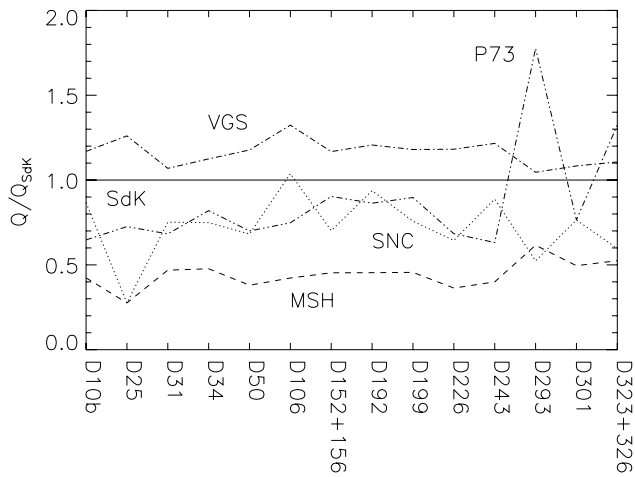


**Figure 2.** Comparison of total predicted  $Q^0$  for each H II region, based on predictions for the observed spectral types of the parent O stars. Line types are as in Figure 1, showing results from different sets of stellar atmosphere models.

using predictions from MSH and SNC for the stellar ionizing outputs. The comparisons consider only observed O stars, and are based on the fully de-reddened spectroscopic classifications used by OK97.

For dwarf O stars, SNC do not provide models for types O5.5, O6, O6.5, O8.5, and O9.5; these types are estimated by simple interpolation between the logarithmic values for which models are presented. Supergiant types not provided by SNC are treated similarly. SNC also do not provide any models for giants, and so these predictions are interpolated between those for luminosity classes V and I. SNC do provide models for both types O9.5 I and O9.7 I, and both are used in our estimates for total  $Q^0$  where applicable; for other sets of models, an observed type O9.7 I is treated as O9.5 I. P73 does not provide predictions for spectral type O3 V and O3 I; for these types we adopted his predictions for type O4 in both cases. For stars where the observed O spectral type is uncertain over a possible range, we adopt the predictions for the latest type. Likewise, if the luminosity class is uncertain, we assume the least luminous in the estimated range. Thus, our total predicted  $Q^0$  are lower limits, in terms of how the uncertainties were carried through in our estimates. This is consistent with the lack of accounting for B stars which provide an additional minor contribution to the ionizing fluxes. Finally, we also caution that WR stars are not included, since their ionizing fluxes are more uncertain, but which may be significant. This analysis is essentially identical to that of OK97, but using the models of SNC and MSH.

Figure 2 compares the total predicted  $Q^0$  of each H II region examined by OK97, adopting predicted ionizing emission rates from the five different studies above. The predictions are compared relative to those of SdK, with line types as in Figure 1. As expected from Figure 1, the predicted aggregate ionizing emission rates are typically 75% and 40% of those predicted by SdK, for SNC and MSH, respectively. Figure 2 also shows some large individual differences in using different sets of models, for example, for DEM 25 and DEM 293. This results from occasional large variations in the predicted properties of individual stars, and underscores the importance of stochastic effects. Objects with fewer stars generally show larger stochastic fluctuations in Figure 2; the last column of Table 1 (below) gives the number of O stars.

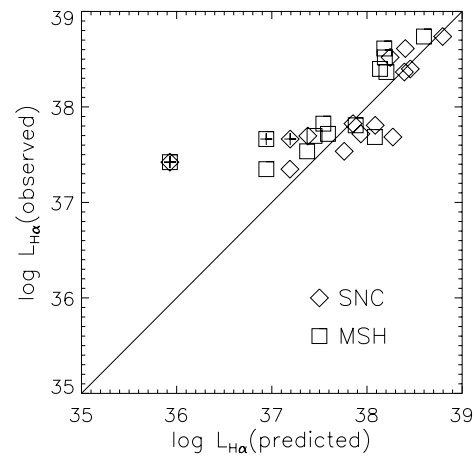


**Figure 3.** Observed versus predicted  $H\alpha$  luminosities for the OK97 sample of H II regions. Diamonds and squares correspond to expected luminosities based on SNC and MSH predictions, respectively. DEM 25 and DEM 50 are marked with crosses; these objects are known to have substantial shock ionization.

Table 1 compares the H II region luminosities with the SNC and MSH predictions. These may be directly compared with similar predictions for P73, VGS, and SdK given by OK97. The first column of Table 1 shows the object name from the Davies et al. (1976; DEM) catalog. Column 2 gives the observed  $H\alpha$  luminosity  $L_{obs}$  from OK97. Columns 3 and 4 give the expected  $H\alpha$  luminosity based on the predicted stellar  $Q^0$ 's from SNC and MSH, respectively, including the effects of reddening based on the color excess  $E(B - V)$  in Column 5. The extinction values and reddening law are the same as those adopted by OK97. Columns 6 and 8 give the ratios of the observed-to-predicted  $H\alpha$  luminosities using the SNC and MSH models, respectively. The numbers of O stars from which the predicted luminosities are derived are given in Column 10.

Because the deviations of these ratios from unity are a multiplicative effect instead of an additive one, characterizations of the aggregate deviation by the mean value are disproportionately skewed by values above unity, e.g., a factor of 2 deviation corresponds to values of 2 and 0.5, yielding a mean of 1.25. OK97 tried to ameliorate this issue by using the median, which works better for asymmetric distributions, but this still does not address the fundamental problem. Instead, we examine the data with a logarithmic analysis, and compute the deviation  $\Delta(\text{SNC})$  of the log luminosities from the relation  $\log L_{obs} = \log L_{SNC}$ , shown in Figure 3. These deviations are given in Column 7 of Table 1, and similarly for the MSH predictions in Column 9. The mean  $\Delta(\text{SNC})$  and  $\Delta(\text{MSH})$  are  $-0.031$  and  $+0.122$ , respectively. These mean deviations in log space thus imply that the observed  $L_{obs}$  are about 93% of those expected by the SNC predictions, while they actually show a factor of 1.33 excess for those of MSH. The standard deviations, adopting SNC and MSH, respectively, are 0.185 and 0.160, or roughly a linear factor of 1.5. We omitted the values for DEM 25 and DEM 50 from these calculations because there is strong evidence that these objects are substantially ionized by supernova shocks (e.g., Oey et al. 2000).

Thus, the aggregate predicted H II region luminosities for SNC and MSH bracket the observed values, and are both well within the standard deviations. It is also worth noting that we used the cooler of the two sets of MSH predictions, and their ‘‘observational scale’’ should agree even better with the observations. Thus, the predicted Lyman continuum emissions

**Table 1**  
Observed and Predicted H II Region Luminosities

H II region	$\log L_{\text{obs}}$	$\log L_{\text{SNC}}$	$L_{\text{MSH}}$	$E(B - V)$	$L_{\text{obs}}/L_{\text{SNC}}$	$\Delta(\text{SNC})$	$L_{\text{obs}}/L_{\text{MSH}}$	$\Delta(\text{MSH})$	$n_*$
DEM 10B	37.8248	37.8531	37.5416	0.16	0.94	-0.02	1.92	0.20	7
DEM 25	37.4216	35.9289	35.9289	0.11	31.10	1.06	31.10	1.06	1
DEM 31	37.8075	38.0864	37.8814	0.09	0.53	-0.20	0.84	-0.05	6
DEM 34	38.7372	38.7952	38.5988	0.10	0.88	-0.04	1.38	0.10	44 <sup>a</sup>
DEM 50	37.6637	37.1931	36.9415	0.12	2.96	0.33	5.27	0.51	3
DEM 106	37.5353	37.7604	37.3711	0.14	0.60	-0.16	1.46	0.12	8
DEM 152+156 <sup>b</sup>	38.3655	38.3927	38.2041	0.10	0.94	-0.02	1.45	0.11	35 <sup>a</sup>
DEM 192	38.3979	38.4548	38.1367	0.09	0.88	-0.04	1.82	0.18	25 <sup>a</sup>
DEM 199	38.6117	38.4031	38.1818	0.05	1.62	0.15	2.69	0.30	22 <sup>a</sup>
DEM 226	37.3483	37.1903	36.9425	0.16	1.44	0.11	2.55	0.29	4
DEM 243	37.7177	37.9355	37.5900	0.10	0.61	-0.15	1.34	0.09	11
DEM 293	37.6964	37.3784	37.4487	0.16	2.08	0.22	1.77	0.18	1
DEM 301	37.6848	38.2718	38.0828	0.06	0.26	-0.42	0.40	-0.28	7
DEM 323+326	38.5185	38.2430	38.1875	0.12	1.89	0.19	2.14	0.23	20

**Notes.**

<sup>a</sup> WR star excluded; DEM 199 contains 3 WR stars.

<sup>b</sup> Not including DEM 152a.

for both SNC and MSH are generally consistent with the observations, suggesting that, systematically, the H II regions appear to be radiation bounded. This result differs from the conclusion of OK97, who found that a significant fraction of the objects appeared to be density bounded. We discuss this more fully in Section 4.

The revised conclusion results primarily from the use of cooler models from SNC and MSH, compared to those of SdK, VGS, and P73 that were used by OK97 (see Figures 1 and 2). Interestingly, the earlier linear, instead of logarithmic, analysis of the ratios of observed-to-predicted luminosities appears to not have significantly biased those results. For example, following the method of OK97, the median  $L_{\text{obs}}/L_{\text{SNC}}$  and  $L_{\text{obs}}/L_{\text{MSH}}$  from Table 1 are 0.94 and 1.77, respectively, excluding DEM 25 and DEM 50. These are in reasonable agreement with our result above of 0.93 for SNC; the agreement with a value of 1.33 for MSH is somewhat less, but recall that the standard deviation is large. OK97 found the median ratio of  $L_{\text{obs}}/L_{\text{SdK}}$  to be 0.74; from Figure 2, we expect the SdK predictions to be roughly 75% those of SNC, thus a median  $L_{\text{obs}}/L_{\text{SdK}}$  of about 0.7 is again fully consistent. However, the agreement may be fortuitous, and the present logarithmic analysis has a stronger fundamental basis.

### 3. A LARGER SAMPLE OF H II REGIONS

The LMC is an ideal candidate galaxy for these detailed studies based on observed and predicted properties of individual massive stars and their nebulae. Since this galaxy is one of our nearest neighbors, and its inclination is nearly face-on, it is possible to observe individual stars and their relation to the surrounding gas without line-of-sight confusion. We now compare predicted and observed ionizing rates for a larger, total sample of 39 LMC H II regions. For this analysis, we chose H II regions that appear isolated in H $\alpha$  observations. We used the continuum-subtracted, flux-calibrated H $\alpha$  image of the LMC from the Southern H $\alpha$  Sky Survey Atlas (SHASSA; Gaustad et al. 2001), cross-correlating with H II regions compiled by Bica et al. (1999), mostly from the well-known DEM and Henize (1956) catalogs. Because the LMC is a small galaxy, the objects in this study represent a significant fraction (~20%) of its bright H II regions. For regions whose associated massive stars

are spectroscopically classified, we can use stellar atmosphere models to predict the ionizing output of the individual OB associations as before. With broadband photometry, we can very roughly estimate spectral types for those stars with no extant spectroscopic data, using the extensive *UBVR* catalog by Massey (2002).

For our sample of 39 objects, we plotted spatial positions, color-magnitude diagrams (CMDs), and H $\alpha$  images with the boundaries overlaid as cataloged by Bica et al. (1999). Figures 4 and 5 are examples of these tools. In each spatial plot, the relative sizes of the symbols indicate the stars' relative brightnesses. The stars denoted with a star symbol are included in Massey's blue catalog, meaning they have  $(B - V)_0 < 0.14$  and  $M_{\text{bol}} < -7.0$ . A comparison of the image and the spatial plot allowed us to determine which stars should be included in our predictions. In general, all stars within the plotted boundary were chosen. However, a comparison of the image to the spatial plot was useful when considering stars at or near the boundary. For example, there is a bright blue star shown (with a star symbol) in the spatial plot for DEM 50 that is right on the northern boundary. We can see from the image that the star is ionizing the hydrogen around it, so we included that star. The CMD also helped to determine how many OB stars we should expect to include.

#### 3.1. H $\alpha$ Ionization Rates

The SHASSA survey has a scale of 47.64 arcsec pixel<sup>-1</sup> and reaches a sensitivity level of 2 Rayleighs ( $1.2 \times 10^{-17}$  erg cm<sup>-2</sup> s<sup>-1</sup> arcsec<sup>-2</sup>) per pixel. The extinction correction used for our observed H $\alpha$  fluxes is based on the flux ratio measurements  $F(\text{H}\alpha)/F(\text{H}\beta)$  by Caplan & Deharveng (1986; hereafter CD86) of individual LMC H II regions. For the nine of our H II regions that overlapped with their sample, we used the values measured by CD86. For the 30 other regions, we used  $F(\text{H}\alpha)/F(\text{H}\beta) = 3.38$ , the average value for the nine regions that overlapped with our sample. This is slightly lower than the average of all 38 of their objects,  $F(\text{H}\alpha)/F(\text{H}\beta) = 3.47$ . The lower value for our sample is reasonable, since we are excluding H II regions in the particularly dusty region around 30 Doradus. To obtain the H $\alpha$  extinction  $A_{\text{H}\alpha}$  from  $F(\text{H}\alpha)/F(\text{H}\beta)$ , we used

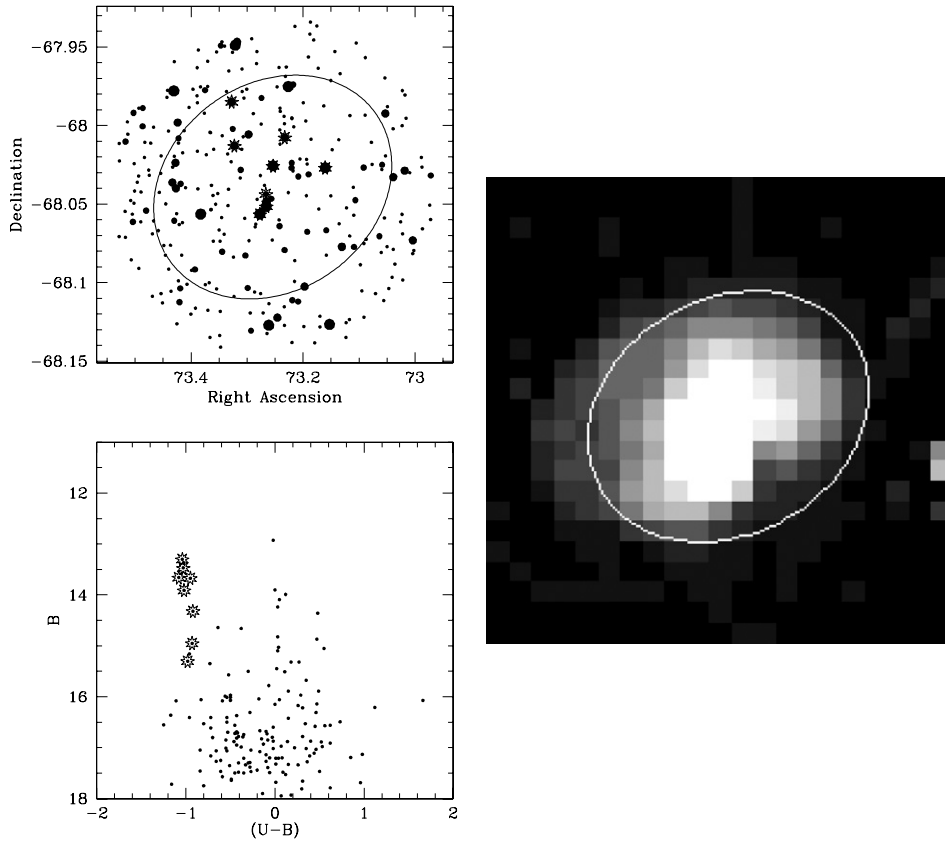


**Figure 4.** Position plot,  $H\alpha$  image, and color–magnitude diagram for DEM 13. We have overlaid the boundary of the  $H\text{ II}$  region as given in Bica et al. (1999). DEM 13 has a major axis of  $10.0'$ , a minor axis of  $8.0'$ , and a position angle of  $120^\circ$ . The relative sizes of the stars in the R.A.–Decl. plot indicate their relative brightnesses. The stars denoted with a star symbol are included in Massey’s blue catalog.

the conversion derived by CD86:

$$A_{H\alpha} = 5.25 \log \left( \frac{F(H\alpha)/F(H\beta)}{2.859} \right). \quad (1)$$

A value of  $F(H\alpha)/F(H\beta) = 3.38$  results in a correction of  $F_{H\alpha, \text{true}} = 1.42 F_{H\alpha, \text{obs}}$ . We checked our measured fluxes for 13  $H\text{ II}$  regions against those of Kennicutt & Hodge (1986) and found good agreement, within 7%. We then converted our measured fluxes to ionizing photon emission rates: assuming an electron temperature of  $T_e = 10,000$  K, we multiplied our  $H\alpha$  photon emission rates by the conversion factor of 2.2 to obtain the corresponding Lyman continuum (LyC) photon emission rates (Hummer & Storey 1987).

### 3.2. Estimating Stellar $Q^0$ From Photometric Data

The  $UBVR$  catalog by Massey (2002) provides photometry for almost 180,000 stars in the LMC. He also provides a compilation of previously published catalogs of about 650 spectral types. We cross-correlated the catalog of stars having spectral types with the  $H\text{ II}$  regions cataloged by Bica et al. (1999), tabulating all known O and B stars, down to spectral type B1.5. We then assigned to each star a predicted  $Q^0$  from the models by SNC, based on its spectral type. Again, we did not include WR stars, since their ionizing outputs are very uncertain. From the CMDs, it was also evident that we were missing spectral types for some of the most massive stars, indicating that we would underestimate the regions’ ionizing output if we did not

supplement the spectroscopy with estimated spectral types (see Table 3, below).

To roughly estimate spectral types from the broadband photometry, we constructed a color–spectral-type calibration using stars that have  $U$  and  $B$  magnitudes having quoted errors less than 0.05 mag and known spectral classifications. We chose  $U - B$  because these bands are closest to the peak of OB stars’ spectral distributions, and therefore the most sensitive to temperature. We corrected the stars’ observed colors for reddening before creating the calibration. Since none of the stars included in the calibration were from  $H\text{ II}$  regions with measured Balmer decrements, we started with the average value used for correcting our  $H\text{ II}$  region fluxes ( $F(H\alpha)/F(H\beta) = 3.38$ ). We used equation (1) to obtain  $A_{H\alpha}$ , and from there, the  $(B - V)$  color excess by

$$A_{H\alpha}/E(B - V) = 2.5, \quad (2)$$

which Parker et al. (1992) interpolated from the relation of Savage & Mathis (1979). Together with the standard ratio  $A_V = 3.1 E(B - V)$ , the average value of  $F(H\alpha)/F(H\beta) = 3.38$  corresponds to  $A_V = 0.47$ . We then assumed that the LMC has an extinction curve similar to that of the Galaxy’s in the visual band, and converted from extinction in  $V$  to extinction in  $U$  and  $B$ . Figure 6 shows our empirical calibration of  $(U - B)_0$  versus spectral type. We mapped the spectral sub-types to a numerical scale and fit a linear relation with the result that the spectral sub-type =  $[(U - B)_0 + 1.255]/0.01$  in our mapping, with about 16% uncertainty in the slope of the line. Figure 6 shows our adopted

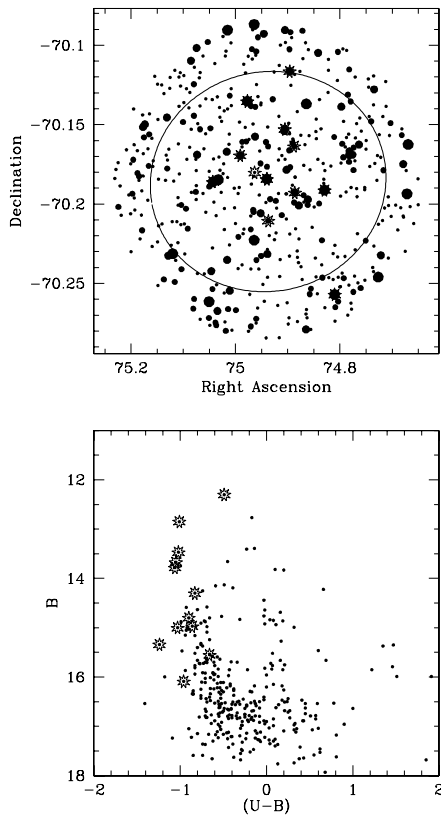


**Figure 5.** Same as Figure 4, for DEM 50. This object has a major axis of  $9.2'$ , a minor axis of  $8.3'$ , and a position angle of  $100^\circ$ .

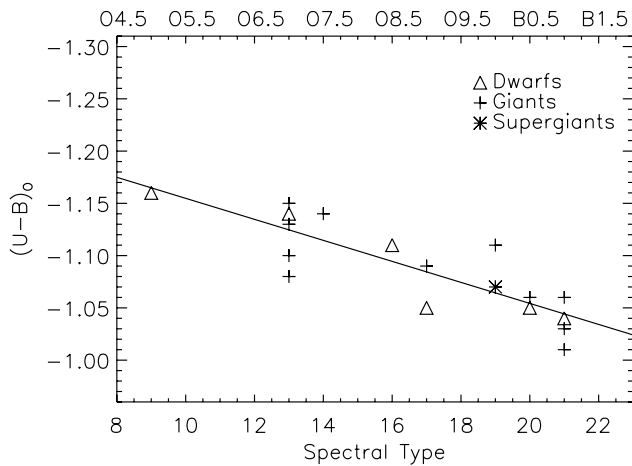
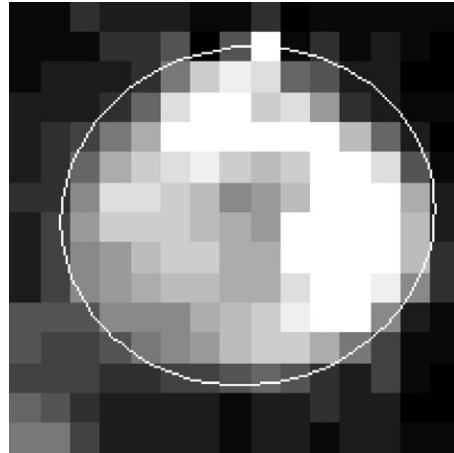


**Figure 6.** Our color-spectral-type calibration for  $U$  and  $B$  photometry. As shown along the top and bottom axes, the spectral sub-types O5, O7.5, and B0 correspond to arbitrary mapped values of 9, 14, and 19, respectively. Triangles, plus signs, and asterisks denote dwarf stars, giants, and supergiants, respectively.

relation. As expected, this relation is unfortunately very shallow, so a small error in  $(U - B)_0$  translates to a large difference in spectral type;  $\delta(U - B)_0 = 0.05$  corresponds to a difference in spectral type of five sub-types.

We used the stars' absolute  $V$  magnitudes,  $M_V$ , to estimate luminosity classes. The extinction correction used to find  $M_V$  from  $V$  is based on  $F(\text{H}\alpha)/F(\text{H}\beta)$  measurements by CD86, but converted to extinction in the visual band as described above. For stars in H II regions with measured Balmer decrements,

$M_V$  was calculated using their H II region's Balmer decrement. Adopting a distance to the LMC of 47.9 kpc (Massey et al. 1995), we derived  $M_V$  for each star. The calibration of MK spectral types with absolute magnitude (Cox 2000) then yielded luminosity classes for those stars for which we estimated spectral types. With estimated spectral types and luminosity classes, we then assigned predicted  $Q^0$  to all the stars for which spectroscopic classifications were unavailable, using the SNC model predictions.

### 3.3. Uncertainties

We summed the predicted ionizing photon emission rates for each H II region in two ways. In the first instance, we used the predicted rates based on spectroscopic classifications and then supplemented with predicted rates for other stars based on photometry. The second method estimates spectral types from photometry for all of the stars, regardless of whether or not spectroscopic classifications were available for any of the stars in the region. This allowed us to test the use of only photometry to estimate spectral types. The pitfalls of using optical photometry to estimate spectral types are well known (e.g. Conti 1986; Massey 1998) and demonstrated above and in Figure 6.

To evaluate how our results are affected by the use of only photometry to estimate the stellar spectral types, we compared our total predicted  $Q^0$  derived in this way to those predicted from spectroscopic classifications plus photometry, for each region. The predicted emission rates are listed in Table 2 for the H II regions for which we have both of these predictions. The second column,  $Q_{\text{SpT+P}}^0$ , is the predicted LyC photon-emission rate derived from spectroscopy plus photometry. The third column,  $Q_{\text{P}}^0$ , is the predicted LyC photon emission rate

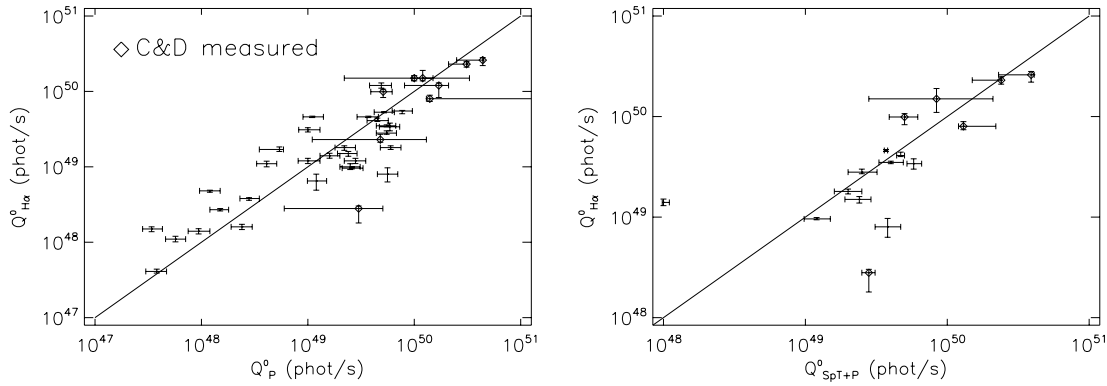


**Figure 7.** Comparison of empirically-derived and predicted ionization rates. Figure 7(a) (left) shows the entire sample, with  $Q^0$  values estimated from photometric data only; Figure 7(b) (right) shows those regions for which  $Q^0$  is predicted from at least some stars with known spectral classifications, and supplemented with photometrically-derived predictions. The line in each plot corresponds to the locus where the two quantities are equal. Diamonds indicate those objects having extinction measurements from CD86.

derived from photometry only. The fourth column is the ratio of these predictions. We find the average ratio  $Q^0_P/Q^0_{SpT+P} = 1.4$ , excluding DEM 25 and DEM 50 for reasons described earlier. Taken at face value, this ratio suggests that, in general, our color-spectral-type calibration tends to type stars earlier than their true classifications, thus overestimating their LyC photon outputs. Therefore, our color-spectral-type calibration appears to give our photometry-only predictions an associated systematic error of about +40%, with a significant uncertainty (Figure 6).

Although both the predicted and empirically-derived ionizing outputs depend on the extinction correction, the ratio of these two values is not as sensitive. To evaluate the uncertainty associated with extinction, we used the  $1\sigma$  deviation from the average  $F(H\alpha)/F(H\beta)$  for the nine regions that were in the CD86 sample. The maximum value of  $F(H\alpha)/F(H\beta)$  for this sample is 3.66 and the minimum is 3.10, corresponding to a range in  $A_V$  of  $A_{V,max} = 0.70$  and  $A_{V,min} = 0.22$ . For the observed  $H\alpha$  luminosities, this means a range in correction factors of 1.22 to 1.91. For stellar predictions, this range of extinction affects the implied stellar luminosity class. The corrections in predicted  $Q^0$  range from a decrease of 21% to an increase of 24%, and for the  $H\alpha$ -inferred  $Q^0$  values, range from a decrease of 17% to an increase of 30%.

Table 3 presents our results for the greater sample. The first column gives the name of the H II region, from its DEM or its Henize (1956) identification. The second column gives the LyC photon emission rate  $Q^0_{H\alpha}$  that corresponds to the observed, extinction-corrected  $H\alpha$  luminosity. Column 3 contains the  $Q^0_P$  predicted from the SNC models using only photometrically estimated spectral types, and Column 4 gives the number of stars from which this is derived. The fifth column gives the deviation  $\Delta(P)$  of the object from the identity relation  $\log Q^0_{H\alpha} = \log Q^0_P$  (Figure 7(a)), and the ratio  $Q^0_{H\alpha}/Q^0_P$  is given in Column 6. Column 7 gives the predicted total LyC emission rate for only stars having spectral classifications, and Column 8 gives the number of these stars. Column 9 presents the  $Q^0_{SpT+P}$  predicted from the SNC models using spectroscopic classifications plus supplementary estimated spectral types from photometry. Column 10 gives the deviation  $\Delta(SpT+P)$  of the object from the relation  $\log Q^0_{H\alpha} = \log Q^0_{SpT+P}$  (Figure 7(b)), and Column 11 gives the ratio  $Q^0_{H\alpha}/Q^0_{SpT+P}$ .

Of the 39 H II regions in this sample, four are also in the OK97 sample, excluding DEM 25 and DEM 50. These objects

**Table 2**  
Comparison of  $Q^0$  Estimated by Photometry Only and Photometry Plus Spectroscopy

H II region	$Q^0_{SpT+P}$	$Q^0_P$	$Q^0_P/Q^0_{SpT+P}$
DEM 6n	$5.0 \times 10^{49}$	$5.1 \times 10^{49}$	1.1
DEM 7	$2.0 \times 10^{49}$	$6.0 \times 10^{49}$	3.0
DEM 9	$2.8 \times 10^{49}$	$3.0 \times 10^{49}$	1.1
DEM 13	$4.7 \times 10^{49}$	$4.5 \times 10^{49}$	1.0
DEM 26	$1.2 \times 10^{49}$	$2.6 \times 10^{49}$	2.2
DEM 55	$3.8 \times 10^{49}$	$5.6 \times 10^{49}$	1.5
DEM 68	$5.8 \times 10^{49}$	$5.9 \times 10^{49}$	1.0
DEM 104	$1.3 \times 10^{50}$	$1.4 \times 10^{50}$	1.1
DEM 192	$8.4 \times 10^{49}$	$1.2 \times 10^{50}$	1.4
DEM 196	$3.7 \times 10^{49}$	$3.7 \times 10^{49}$	1.0
N 138	$4.0 \times 10^{49}$	$5.5 \times 10^{49}$	1.4
DEM 199	$3.9 \times 10^{50}$	$4.4 \times 10^{50}$	1.1
DEM 229	$2.4 \times 10^{50}$	$3.1 \times 10^{50}$	1.3
DEM 250	$2.4 \times 10^{49}$	$2.4 \times 10^{49}$	1.0

are DEM 31, DEM 192, DEM 199, and DEM 226. The OK97 spectral classifications were not included in the Massey catalog, and so we used only photometry to estimate the spectral types of most of the stars in these regions. This offers another test and quantitative insight on the uncertainties associated with the photometric method of estimating spectral types. Comparing the ratios of  $Q^0_{H\alpha}/Q^0_P$  in Table 3 to those of  $L_{obs}/L_{SNC}$  in Table 1 for these four objects, there is a large scatter, consistent with the variations seen in Table 2. For example, the comparison suggests that unaccounted-for stars are a factor for both separate analyses.

Other contributions to the random uncertainties stem from those associated with the  $H\alpha$  measurements and having incomplete spectroscopy or photometry in a given H II region. However, our total systematic uncertainty is likely dominated by our color-spectral-type calibration.

### 3.4. Observed Versus Predicted Ionization Rates

Figure 7 shows the comparison of empirically-derived  $Q^0$  values and predicted values for this sample. Figure 7(a) shows the comparison of  $Q^0_{H\alpha}$  to  $Q^0_P$  for all 39 H II regions. The predicted ionizing rates are based solely on estimated spectral types from photometry (Column 3 from Table 3). Figure 7(b) shows the 16 objects for which we had at least one star spectroscopically classified, plotting the predicted LyC photon emission rates

**Table 3**  
Lyman Continuum Emission Rates for a Larger Sample of H II Regions<sup>a</sup>

Name	$Q_{\text{H}\alpha}^0$ ( $\text{s}^{-1}$ )	$Q_{\text{P}}^0$ ( $\text{s}^{-1}$ )	$N_{\text{P}}$	$\Delta(\text{P})$	$Q_{\text{H}\alpha}^0/Q_{\text{P}}^0$	$Q_{\text{SpT}}^0$ ( $\text{s}^{-1}$ )	$N_{\text{SpT}}$	$Q_{\text{SpT+P}}^0$ ( $\text{s}^{-1}$ )	$\Delta(\text{SpT+P})$	$Q_{\text{H}\alpha}^0/Q_{\text{SpT+P}}^0$
DEM 1	$4.1 \times 10^{+47}$	$3.8 \times 10^{+47}$	1	0.02	1.1	...	0	...	...	...
DEM 2	$1.4 \times 10^{+48}$	$9.4 \times 10^{+47}$	1	0.12	1.5	...	0	...	...	...
DEM 4	$4.6 \times 10^{+49}$	$1.1 \times 10^{+49}$	11	0.44	4.2	...	0	...	...	...
DEM 6n	$9.9 \times 10^{+49}$	$5.1 \times 10^{+49}$	42	0.20	1.9	$1.3 \times 10^{+47}$	2	$5.0 \times 10^{+49}$	0.21	2.0
DEM 7	$1.8 \times 10^{+49}$	$6.0 \times 10^{+49}$	11	-0.37	0.30	$1.3 \times 10^{+47}$	2	$2.0 \times 10^{+49}$	-0.03	0.90
DEM 9	$2.8 \times 10^{+48}$	$3.0 \times 10^{+49}$	2	-0.73	0.09	$2.5 \times 10^{+49}$	1	$2.8 \times 10^{+49}$	-0.71	0.10
DEM 11	$1.2 \times 10^{+49}$	$2.8 \times 10^{+49}$	6	-0.26	0.43	...	0	...	...	...
DEM 13	$4.1 \times 10^{+49}$	$4.5 \times 10^{+49}$	11	-0.03	0.91	$3.4 \times 10^{+49}$	4	$4.7 \times 10^{+49}$	-0.04	0.87
DEM 14	$1.5 \times 10^{+48}$	$3.4 \times 10^{+47}$	1	0.46	4.4	...	0	...	...	...
DEM 15a	$4.8 \times 10^{+48}$	$1.2 \times 10^{+48}$	4	0.43	4.0	...	0	...	...	...
DEM 15	$3.1 \times 10^{+49}$	$1.0 \times 10^{+49}$	17	0.35	3.1	...	0	...	...	...
DEM 22	$1.2 \times 10^{+50}$	$1.7 \times 10^{+50}$	28	-0.11	0.71	...	0	...	...	...
DEM 25	$1.4 \times 10^{+49}$	$1.6 \times 10^{+49}$	4	...	0.88	$7.9 \times 10^{+47}$	1	$1.0 \times 10^{+48}$	...	14
DEM 26	$9.6 \times 10^{+48}$	$2.6 \times 10^{+49}$	7	-0.31	0.37	$8.9 \times 10^{+47}$	2	$1.2 \times 10^{+49}$	-0.07	0.80
DEM 31	$5.5 \times 10^{+49}$	$7.7 \times 10^{+49}$	30	-0.10	0.71	...	0	...	...	...
DEM 32	$1.6 \times 10^{+48}$	$2.4 \times 10^{+48}$	4	-0.12	0.67	...	0	...	...	...
DEM 33	$1.1 \times 10^{+49}$	$4.1 \times 10^{+48}$	1	0.30	2.7	...	0	...	...	...
N 92	$1.0 \times 10^{+49}$	$2.5 \times 10^{+49}$	6	-0.28	0.40	...	0	...	...	...
DEM 50	$2.8 \times 10^{+49}$	$5.5 \times 10^{+49}$	14	...	0.51	$5.3 \times 10^{+47}$	2	$2.5 \times 10^{+49}$	...	1.1
DEM 55	$8.0 \times 10^{+48}$	$5.6 \times 10^{+49}$	16	-0.60	0.14	$7.9 \times 10^{+47}$	1	$3.8 \times 10^{+49}$	-0.48	0.21
DEM 68	$3.4 \times 10^{+49}$	$5.9 \times 10^{+49}$	28	-0.17	0.58	$2.6 \times 10^{+49}$	5	$5.8 \times 10^{+49}$	-0.16	0.59
DEM 84	$5.3 \times 10^{+49}$	$5.2 \times 10^{+49}$	28	0.01	1.0	...	0	...	...	...
DEM 86	$1.5 \times 10^{+50}$	$1.0 \times 10^{+50}$	36	0.12	1.5	...	0	...	...	...
DEM 103	$3.8 \times 10^{+48}$	$2.8 \times 10^{+48}$	2	0.09	1.4	...	0	...	...	...
DEM 104	$8.0 \times 10^{+49}$	$1.4 \times 10^{+50}$	38	-0.17	0.57	$8.9 \times 10^{+47}$	2	$1.3 \times 10^{+50}$	-0.15	0.62
DEM 128	$1.1 \times 10^{+48}$	$5.7 \times 10^{+47}$	2	0.20	1.9	...	0	...	...	...
DEM 134	$1.2 \times 10^{+50}$	$4.9 \times 10^{+49}$	37	0.28	2.4	...	0	...	...	...
DEM 157	$2.7 \times 10^{+48}$	$1.5 \times 10^{+48}$	3	0.18	1.8	...	0	...	...	...
DEM 174	$1.8 \times 10^{+49}$	$2.2 \times 10^{+49}$	7	-0.06	0.82	...	0	...	...	...
DEM 178	$6.5 \times 10^{+48}$	$1.2 \times 10^{+49}$	5	-0.19	0.54	...	0	...	...	...
DEM 192	$1.5 \times 10^{+50}$	$1.2 \times 10^{+50}$	60	0.07	1.3	$1.1 \times 10^{+49}$	5	$8.4 \times 10^{+49}$	0.18	1.8
DEM 196	$4.6 \times 10^{+49}$	$3.7 \times 10^{+49}$	14	0.07	1.2	$3.2 \times 10^{+49}$	1	$3.7 \times 10^{+49}$	0.07	1.2
N 138	$3.5 \times 10^{+49}$	$5.5 \times 10^{+49}$	19	-0.14	0.64	$3.2 \times 10^{+48}$	2	$4.0 \times 10^{+49}$	-0.04	0.88
DEM 197	$2.3 \times 10^{+49}$	$4.8 \times 10^{+49}$	21	-0.23	0.48	...	0	...	...	...
DEM 199	$2.6 \times 10^{+50}$	$4.4 \times 10^{+50}$	94	-0.16	0.59	4.4E+46	2	$3.9 \times 10^{+50}$	-0.12	0.67
N 148C	$1.2 \times 10^{+49}$	$1.0 \times 10^{+49}$	4	0.06	1.2	...	0	...	...	...
DEM 226	$1.7 \times 10^{+49}$	$5.4 \times 10^{+48}$	6	0.35	3.1	...	0	...	...	...
DEM 229	$2.3 \times 10^{+50}$	$3.1 \times 10^{+50}$	109	-0.09	0.74	$2.2 \times 10^{+48}$	7	$2.4 \times 10^{+50}$	-0.01	0.96
DEM 250	$1.5 \times 10^{+49}$	$2.4 \times 10^{+49}$	11	-0.14	0.63	1.3E+46	1	$2.4 \times 10^{+49}$	-0.14	0.63

**Note.** <sup>a</sup> See Section 3.3 for a description of the tabulated quantities.

supplemented by the photometry-based predictions,  $Q_{\text{SpT+P}}^0$  (Column 9 of Table 3). The plots include a reference line indicating the locus where  $Q_{\text{H}\alpha}^0$  equals the predicted LyC photon emission rate. The nine regions with  $F(\text{H}\alpha)/F(\text{H}\beta)$  measurements by CD86 are designated by diamonds.

In Figure 7, the data are plotted as error bars, to demonstrate the relative importance of measurement uncertainties. The error bars for  $Q_{\text{H}\alpha}^0$  are based on our uncertainty in the determination of the H $\alpha$  background for each individual region: if the uncertainty was less than 8%, then we used an error of 8%, the rms error in the calibration of the H $\alpha$  image as quoted by Gaustad et al. (2001). The error bars for the predicted LyC photon emission rates were found by changing the extinction corrections for each region, as described in Section 3.3. Again, we emphasize that the error bars show the H $\alpha$  measurement uncertainties only, and do not include the much larger systematic uncertainties due to the stellar atmosphere models, using photometry to classify stars, and stars that are unaccounted for.

We follow our analysis in Section 2.1, and evaluate the deviation of the data in Figure 7 from the identity relation. The mean  $\Delta(\text{P}) = -0.014$  for the larger sample, with  $\sigma = 0.273$ .

These values correspond to a linear  $Q_{\text{H}\alpha}^0/Q_{\text{P}}^0 = 0.97$  with a characteristic scatter of a factor of 1.88. For the subsample that include some spectral classifications (Figure 7(b)), we obtain a mean  $\Delta(\text{SpT+P}) = -0.106$ , with  $\sigma = 0.240$ , yielding  $Q_{\text{H}\alpha}^0/Q_{\text{SpT+P}}^0 = 0.78$  and scatter of 1.74. For comparison, the median values for  $Q_{\text{H}\alpha}^0/Q_{\text{P}}^0$  and  $Q_{\text{H}\alpha}^0/Q_{\text{SpT+P}}^0$  are 0.86 and 0.84, respectively. As before, these calculations omit the data for DEM 25 and DEM 50.

#### 4. DISCUSSION AND CONCLUSION

We have emphasized that the results from the comparison of the larger sample in Section 3 have much more intrinsic uncertainty than those in Section 2, where we based the analysis on fairly complete spectroscopic classifications from OK97. Nevertheless, the results for the two samples are in excellent agreement, and so the larger sample helps to better establish these results. For the OK97 sample, we found in Section 2 that the characteristic ratio of observed-to-predicted H $\alpha$  luminosities is 0.93, with a factor of 1.5 scatter; for the new, larger sample

in Section 3, the ratio of observed-to-predicted  $Q^0$  is 0.97, with a factor of 1.9 scatter; and for the subsample of 14 objects having some stars with spectroscopic data, the relative ratio is 0.78, with a factor of 1.7 scatter. All of the above values use the SNC predictions for stellar LyC emission. The agreement is rather remarkable, perhaps fortuitous, and well within the uncertainties, both observational and systematic.

Our results for all the datasets considered here therefore indicate that, based on the new SNC and MSH model atmospheres, *the H II regions are generally consistent with radiation bounding*. This result contrasts with our findings a decade ago (OK97), based on the SdK models, for which we suggested that about 50% of ionizing radiation escapes the classical H II regions and ionizes the WIM. When comparing our Table 1 with Table 2 from OK97, the more recent SNC and MSH fluxes reduce the predicted nebular luminosities and bring several of the seemingly density-bounded regions in general agreement with being radiation bounded. This is especially the case for the MSH predictions. Nevertheless, there are some objects which remain convincingly density bounded, in particular, DEM 31 and DEM 301. DEM 106 may also be density bounded, depending on which set of predictions is more accurate. All three of these objects show strong shell-like and filamentary morphology (e.g., Oey 1996), which is highly conducive to the escape of radiation. The shock-excited objects, DEM 25 and DEM 50 have extremely similar morphology and are also most likely density bounded, even though our analysis cannot evaluate this possibility because of the overionization by shocks.

It is therefore apparent that the large dispersion in the results is caused not only by random and non-random errors, but also by real scatter. It is difficult to evaluate the relative importance of each, and it still remains possible that a significant quantity of LyC radiation does systematically escape from the H II regions. The preceding discussion suggests that 20–30% of the objects in the OK97 sample, and perhaps more, appear to be density bounded. This is less than the estimate of 50% suggested by OK97, but still a significant fraction. We also recall that the predicted total  $Q^0$  for the objects are lower limits because of the omission of WR stars, early B stars, and occasional, unaccounted-for O stars. We note that while the SNC models may appear to have the best agreement with the observations at face value, the MSH models may turn out to be the most realistic when considering the nature of the predictions as lower limits.

In considering the global net effect of the different model predictions, we can evaluate the total observed and total predicted nebular luminosities for the entire sample, as done by Hoopes & Walterbos (2000). While this method is biased toward the brightest individual objects, it does capture the total aggregate effects. For the OK97 sample, the ratios of the observed total luminosities to those predicted from the MSH and SNC models are  $L_{\text{obs}}(\text{tot})/L_{\text{MSH}}(\text{tot}) = 1.62$ , and  $L_{\text{obs}}(\text{tot})/L_{\text{SNC}}(\text{tot}) = 1.01$ , respectively. For comparison, the SdK predictions yield  $L_{\text{obs}}(\text{tot})/L_{\text{SdK}}(\text{tot}) = 0.76$ . This again shows that the earlier models provided for excess LyC radiation which would be available to ionize the WIM, whereas the latest models do not. We again note that, although the aggregate predictions from the MSH atmospheres appear to underpredict the observations, we chose their “theoretical scale” models indeed because of their more extreme variation, and that their “observational scale” predictions will be more consistent with the observations, especially when considering the that our tabulation of the predictions are lower limits.

In summary, our results are consistent with the majority of the H II regions being radiation bounded. These results complicate the scenario for the ionization of the WIM. The study of massive field stars in M33 (Hoopes & Walterbos 2000) suggested that field stars alone cannot provide the ionizing photons necessary to create and maintain the WIM. Specifically, that study found that the ionization requirement for the WIM is about 40% of that of the H II regions. Field OB stars can account for about half of this ionization requirement of the WIM, and the remaining 50% would require H II regions to leak about 20–25% of the ionizing photons. The comparison of predicted-to-observed ionization rates for H II regions for M33 could barely meet this requirement for leakage; on average, for the H II regions in the Hoopes & Walterbos study, the ratio of predicted-to-observed  $Q^0$  was  $1.07 \pm 0.26$ . With the newer predictions for ionizing photon rates from massive stars, their predicted rates would also likely decrease. Similarly, the earlier results from OK97 also indicated that LyC photons leaking from H II regions are a likely source for the diffuse ionization. If these results are borne out, it may be necessary to consider additional ionizing sources for the WIM, for example, heating by turbulence (e.g., Minter & Spangler 1997; Slavin et al. 1993), the extragalactic radiation field (Reynolds et al. 1995), or more exotic mechanisms. However, further examination of the LyC photon budget in star-forming galaxies is necessary to evaluate whether there is a significant discrepancy in ionization sources for the WIM.

We acknowledge support from the NASA Astrophysics Data Program, grant NAG5-10768. We thank Wayne Landsman and Joel Parker for providing and recalibrating data from *UIT*, which we unsuccessfully attempted to use in an earlier analysis for this work. M.S.O. and T.M.W. also acknowledge support from the NSF, grant AST-0448893. Thanks also to Claus Leitherer for useful discussions and an anonymous referee for insightful comments.

## REFERENCES

- Auer, L. H., & Mihalas, D. 1972, *ApJS*, **24**, 193  
 Bianchi, L., & Garcia, M. 2002, *ApJ*, **581**, 610  
 Bica, E. L. D., Schmitt, H. R., Dutra, C. M., & Oliveira, H. L. 1999, *AJ*, **117**, 238  
 Bradley, P. T., & Morton, D. C. 1969, *ApJ*, **156**, 687  
 Caplan, J., & Deharveng, L. 1986, *AAP*, **155**, 297 (CD86)  
 Conti, P. S. 1986, in *IAU Symp 116, Luminous Stars and Associations in Galaxies*, ed. C. W. H. de Loore, A. J. Willis, & P. Laskarides (Dordrecht: Reidel), 199  
 Cox, A. N. 2000, *Allen’s Astrophysical Quantities*, 4th Ed. (New York: AIP Press)  
 Crowther, P. A. 1998, in *IAU Symp. 183, Fundamental Stellar Properties*, ed. T. R. Bedding, A. J. Booth, & J. Davis (San Francisco, CA: ASP), 137  
 Davies, R. D., Elliott, K. H., & Meaburn, J. 1976, *MmRAS*, **81**, 89 (DEM)  
 Ferguson, A. M. N., Wyse, R. F. G., Gallagher, J. S. III, & Hunter, D. A. 1996, *AJ*, **111**, 2265  
 Gaustad, J. E., McCullough, P. R., Rosing, W., & Van Buren, D. 2001, *PASP*, **113**, 1326  
 Henize, K. G. 1956, *ApJS*, **2**, 315  
 Heap, S. R., Lanz, T., & Hubeny, I. 2006, *ApJ*, **638**, 409  
 Hillier, D. J., & Miller, D. L. 1998, *ApJ*, **496**, 407  
 Hoopes, C. G., & Walterbos, R. A. M. 2000, *ApJ*, **541**, 597  
 Hoopes, C. G., Walterbos, R. A. M., & Greenwalt, B. E. 1996, *AJ*, **112**, 1429  
 Hummer, D. G., & Storey, P. J. 1987, *MNRAS*, **224**, 801  
 Hunter, D. A., & Massey, P. 1990, *AJ*, **99**, 846  
 Kennicutt, R. C. Jr., & Hodge, P. W. 1986, *ApJ*, **306**, 130  
 Kudritzki, R. P. 2002, *ApJ*, **577**, 389

- Kurucz, R. L. 1992, in IAU Symp. 149, The Stellar Populations of Galaxies, ed. B. Barbuy, & A. Renzini (Dordrecht: Kluwer), 225
- Lanz, T., & Hubeny, I. 2003, *ApJS*, 146, 417
- Leitherer, C., et al. 1999, *ApJS*, 123, 3
- Martins, F., Schaerer, D., & Hillier, D. J. 2005, *A&A*, 436, 1049 (MSH)
- Massey, P. 1998, in Stellar Astrophysics for the Local Group, ed. A. Aparicio, A. Herrero, & F. Sanchez (Cambridge: Cambridge Univ. Press), 95
- Massey, P. 2002, *ApJS*, 141, 81
- Massey, P., Lang, C. C., Degioia-Eastwood, K., & Garmany, C. D. 1995, *ApJ*, 438, 188
- Massey, P., Puls, J., Pauldrach, A. W. A., Bresolin, F., Kudritzki, R. P., & Simon, T. 2005, *ApJ*, 627, 477
- Minter, A. H., & Spangler, S. R. 1997, *ApJ*, 485, 182
- Mokiem, M. R., Martín-Hernández, N. L., Lenorzer, A., de Koter, A., & Tielens, A. G. M. 2004, *A&A*, 419, 319
- Mokiem, M. R., et al. 2006, *A&A*, 456, 1131
- Mokiem, M. R., et al. 2007, *A&A*, 465, 2007
- Morisset, C., Schaerer, D., Bouret, J. C., & Martins, F. 2004, *A&A*, 415, 577
- Morton, D. C. 1969, *ApJ*, 158, 629
- Oey, M. S. 1996, *ApJ*, 465, 231
- Oey, M. S., Dopita, M. A., Shields, J. C., & Smith, R. C. 2000, *ApJS*, 128, 511
- Oey, M. S., & Kennicutt, R. C., Jr. 1997, *MNRAS*, 291, 827 (OK97)
- Panagia, N. 1973, *AJ*, 78, 929 (P73)
- Parker, J. W., Garmany, C. D., Massey, P., & Walborn, N. R. 1992, *AJ*, 103, 1205
- Pauldrach, A. W. A., Hoffmann, T. L., & Lennon, M. 2001, *A&A*, 375, 161
- Repolust, T., Puls, J., & Herrero, A. 2004, *A&A*, 415, 349
- Reynolds, R. J., Tufte, S. L., Kung, D. T., McCullough, P. R., & Heiles, C. 1995, *ApJ*, 448, 715
- Savage, B. D., & Mathis, J. S. 1979, *ARA&A*, 17, 73
- Schaerer, D., & de Koter, A. 1997, *A&A*, 322, 598 (SdK)
- Slavin, J. D., Shull, J. M., & Begelman, M. C. 1993, *ApJ*, 407, 83
- Smith, L. J., Norris, R. P. F., & Crowther, P. A. 2002, *MNRAS*, 337, 1309 (SNC)
- Vacca, W. D., Garmany, C. D., & Shull, J. M. 1996, *ApJ*, 460, 914 (VGS)
- Van Citters, G. W., & Morton, D. C. 1970, *ApJ*, 161, 695